Liquid phase aldol condensation reactions with MgO–ZrO$_2$ and shape-selective nitrogen-substituted NaY

Wenqin Shen[a], Geoffrey A. Tompsett[a], Karl D. Hammond[a], Rong Xing[a], Fulya Dogan[b], Clare P. Grey[b], W. Curtis Conner Jr.[a], Scott M. Auerbach[a,c], George W. Huber[a,*]

[a] Department of Chemical Engineering, University of Massachusetts, 686 N. Pleasant St, Amherst, MA 01003-3110, United States
[b] Department of Chemistry, State University of New York at Stony Brook, Stony Brook, NY 11794-3400, United States
[c] Department of Chemistry, University of Massachusetts, Amherst, MA 01003-9336, United States

ARTICLE INFO

ABSTRACT

The aldol condensation reactions of furfural/hydroxymethylfurfural (furfurals) with acetone/propanal in water–methanol solvents were studied over the solid base catalysts MgO–ZrO$_2$, NaY and nitrogen-substituted NaY (Nit-NaY). The reactions were conducted at 120 °C and 750 psig of He in batch reactors. Nit-NaY exhibited catalytic activity for aldol condensation comparable to MgO–ZrO$_2$ and much higher than that of NaY, indicative of the increased base strength after replacing the bridging oxygen with the lower electronegativity nitrogen over Nit-NaY. The aldol condensation of furfurals with acetone produces two different products, the monomer and the dimer. The monomer is formed from reaction of furfurals with acetone. The dimer is formed from reaction of the monomer with furfurals. MgO–ZrO$_2$ had a higher selectivity towards dimer formation. In contrast, Nit-NaY was more selective towards the monomer product due to the cage size in the FAU structure, indicating that Nit-NaY is a shape selective base catalyst. Increasing the water concentration in the feed solution or increasing the feed concentration led to both increased catalytic activity and dimer selectivity. The Nit-NaY catalyst was not stable and lost catalytic activity when recycled due to leaching of the framework nitrogen. Different characterization techniques, including XRD, high resolution Ar adsorption isotherm, basic sites titration, CO$_2$ TPD-MS, TGA and ^{29}Si SP MAS NMR, were used here to characterize the fresh and spent catalysts. The results show that Nit-NaY maintains only part of the FAU-type crystal structure. Furthermore, the base strength over Nit-NaY was found to be between that of Mg^{2+}–O^{2-} pair and Mg(OH)$_2$. The reaction mechanism over Nit-NaY was discussed.

1. Introduction

Solid base catalysts have attracted much attention because of their potential to replace corrosive homogeneous base catalysts in industrially important reactions such as isomerizations, alkylations, condensations, additions, cyclizations, transesterifications and oxidations [1–5]. The use of solid catalysts provides a more environmentally benign process and reduces the cost of processing due to the ease of separation and recycling. Base strength, stability, and shape or size selectivity are the most desired properties for solid base catalysts. Shape selective acidic zeolites are the backbone of the petroleum industry [6]. However, shape selective basic catalysts have not been used commercially yet. Basic nanoporous materials can be prepared by various methods including ion-exchange with alkali metal cations [5,7], impregnation or occlusion with basic salts or metals [8–11], organic base grafting [12–15] and nitridation [16–23]. These methods all have their limitations for preparing shape-selective basic zeolites. For example, ion-exchange methods produce only weak bases [24]. Impregnation or occlusion may cause the blockage of zeolite pores [25]. Organic base grafting may only modify the basicity of the surface or cause the blockage of the micropores of zeolites due to the large organic groups, and thereby does not produce the desired shape selectivity [26–28]. Nitridation of zeolites has been discussed as a promising option for the generation of truly shape selective base catalysts [29,30]. Nitrided zeolites have been prepared by treating zeolites with ammonia at elevated temperatures. This results in an increased base strength of the framework due to the substitution of bridging oxygen with the lower electronegativity nitrogen [29,30]. Nitridation has been performed on a range of porous materials including mesoporous MCM-41 [31–33] and SBA-15 [34,35], aluminophosphates (AlPOs) [17,36], silicon substituted aluminophosphates (SAPOs) [37,38] and zeolites [17,18,39,40]. The nitrogen-substituted materials have been evaluated by Knoeve-
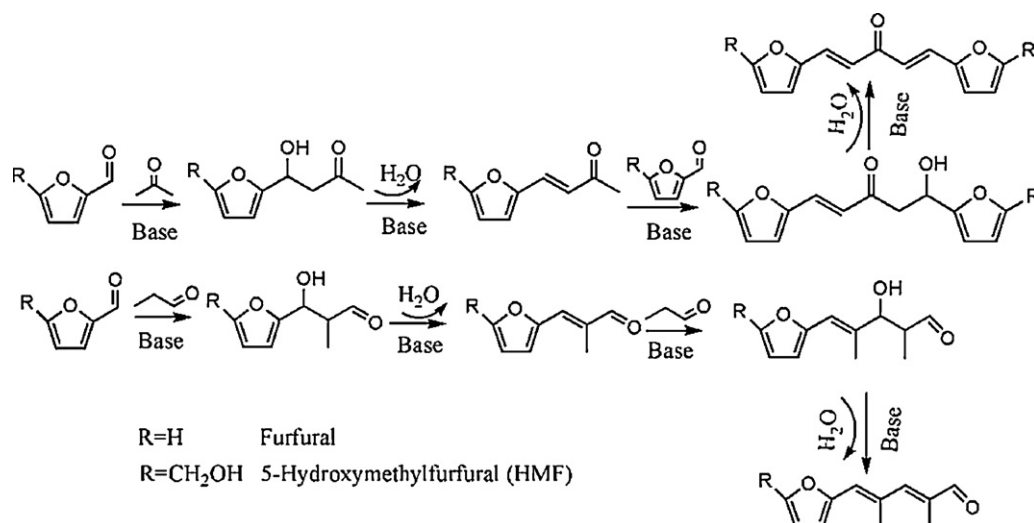
Scheme 1. Base catalyzed aldol condensation of furfurals with acetone or propanal.

nagel condensations of benzaldehyde with molecules containing active methylenic groups with different pK_a values and showed basic activity and stability [17,18,32,36,38,40]. However, there are no reports on the shape selectivity over these nitrogen-substituted materials.

A sustainable biomass economy requires the development of different integrated steps for the conversion of biomass-derived feedstocks into a range of fuels and chemicals [41]. Many of these steps involve basic catalysts. One key step in a biorefinery concept to produce diesel and jet fuel range alkanes involves C–C bond forming reactions by aldol condensations. Biomass can be depolymerized into C5 and C6 sugars by hydrolysis-based approaches. However, to make diesel and jet fuel range alkanes that are between C8 to C15, C–C bond forming reactions must occur. One approach to form these larger alkanes involves first a dehydration step to produce furfurals. The furfurals are then reacted with an aldehyde or ketone by aldol condensation to form C8 to C15 alkane precursors. These larger compounds then undergo hydrodeoxygenation reactions to produce the final alkanes [42–45]. Base catalysis is the key step in C–C bond forming reactions to produce the chemicals or fuels with targeted molecular weight.

The products from the condensation of furfural with acetone or propanal are shown in Scheme 1. 5-Hydroxymethyl furfural (HMF) will undergo the same chemistry as furfural. Acetone reacts with one molecule of furfural (or HMF) to form furfural (or HMF) acetone monomer 4-(2-furyl)-3-buten-2-one (or 4-[5-(hydroxymethyl)-2-furanyl]-3-buten-2-one), followed by condensation with another furfural (or HMF) to form furfural (or HMF) acetone dimer 1,5-di-2-furanyl-1,4-pentadien-3-one (or 1,5-bis[(5-hydroxlmethyl)-2-furanyl]-1,4-pentadien-3-one). Propanal reacts with one furfural (or HMF) to form furfural (or HMF) propanal monomer 3-(2-furyl)-2-methylacrolein (or 3-[(5-hydroxymethyl)-2-furanyl]-2-methylacrolein) and the monomer can further react with another propanal molecule to produce furfural (or HMF) propanal dimer 5-(2-furyl)-2,4-dimethyl-2,4-pentadienal (or 5-[(5-hydroxlmethyl)-2-furyl]-2,4-dimethyl-2,4-pentadienal).

Aldol condensation of furfurals with acetone has been studied in homogeneous ethanol/water solutions [46] and water/THF biphasic system [42] catalyzed by NaOH. It has also been studied in aqueous solutions catalyzed by solid base catalysts followed by hydrogenation [43] and the combined aldol condensation with hydrogenation over bi-functional catalyst 5 wt.% Pd/MgO–ZrO2 [44]. MgO–ZrO2 showed the highest catalytic activity and excellent recycling ability compared with other solid base catalysts such as MgO, CaO, Mg–Al-oxide, and MgO/ZrO2 prepared by impregnation. However, there is no preference to the monomer or the dimer product by using either homogeneous NaOH or the heterogeneous MgO–ZrO2 catalyst. This paper will present the first report to apply nitrogen-substituted NaY for the reactions from bio-renewable sources to generate value-added chemicals and fuels. The objectives of this research are (1) to demonstrate the increased catalytic activity by nitrogen substitution over NaY using aldol condensation of furfurals with acetone or propanal as probe reactions and (2) to demonstrate that the nitrogen substituted zeolites can be shape selective base catalysts. The Nit-NaY catalyst will be compared with the known non-shape selective MgO–ZrO2 catalyst using different reaction conditions.

2. Experimental

2.1. Catalyst preparation

MgO–ZrO2 was prepared by precipitation of Mg(NO3)2·6H2O (Aldrich) and ZrO(NO3)2·6H2O (Aldrich) aqueous solution with NaOH as described elsewhere [44,47,48]. Typically, 50.9 g of magnesium nitrate and 4.04 g zirconyl nitrate were dissolved in 1 L of deionized water. A 25 wt.% NaOH aqueous solution in a separation funnel was dropped into the mixed solution with vigorous stirring until the pH was equal to 10 as monitored by a pH meter. The resulting gel was aged at room temperature for 72 h and separated by vacuum filtration. The precipitate was thoroughly washed with deionized water at least four times and dried in an oven at 120 °C overnight. The MgO–ZrO2 catalyst was obtained by calcination of the resulting dry precipitate in 100 mL/min air flow at 600 °C for 3 h with a 3 h heating ramp. NaY (CBV100 with a Si/Al ratio of 2.55, Zeolyst International) was used as a starting material to prepare nitrogen-substituted NaY. In a typical synthesis, about 5 g NaY was loaded into a quartz tube with a 1 in. outer diameter supported by a quartz frit. Before nitridation, NaY was first dried under a flow of 100 mL/min nitrogen at 110 °C for 2 h with a 0.5 °C/min ramp rate, and then dehydrated at 400 °C for 6 h with a 0.5 °C/min ramp rate. It was found by us previously that high ammonia flow rates are crucial for substantial nitrogen substitution while maintaining acceptable microporosity and crystallinity [21]. The NaY was nitrided in a flow of 1 L/min ammonia (Airgas, anhydrous, 99.99%) at 850 °C with a 1.5 °C/min ramp for 24 h. A slow heating rate was used here to remove water gradually and avoid dealumination of the zeolite [22]. The resulting material was cooled to room tem-

perature under nitrogen flow and stored in a desiccator, labeled as Nit-NaY.

2.2. Catalytic reaction and analysis methods

The catalysts were evaluated in a high throughput parallel automatic reactor system (CAT 24, HEL Group). The system temperature, pressure, and gas flow rate were controlled and monitored through WinISO E670 software. In a typical run, 2 mL reactant solution, a suitable amount of catalyst, and a stir bar were put into a glass tube reactor with a total capacity of 3 mL. All of the prepared glass tube reactors (maximum 24) were loaded into a high pressure chamber. Inside the chamber, stainless steel cooling tips were inserted into the top of each glass tube, effectively preventing the mixing of vapor between glass reactors. Before starting the reaction, the chamber was purged with helium for 10 min and pressurized to 500 psig. Next, the chamber was heated to 120 °C. More helium was introduced to maintain the final pressure at 750 psig. The reaction was kept at 120 °C for 16 h or 24 h and stirred at 850 rpm. After reaction, the whole chamber was quenched in an ice bath immediately to stop the reaction. The resulting mixture inside each glass tube reactor was transferred to a 25 mL sample bottle. The glass reactor was washed three times with methanol (HPLC grade) to dissolve the products deposited on the glass wall. Samples for HPLC analysis were filtered by a syringe filter (Waters 0.45 μm PES syringe membrane filter).

The stability test was conducted in a Parr batch reactor (model #4566) with an external temperature and stirring controller (Model #4835). A 75 mL reactant solution (5 wt.% total organics, furfural/acetone = 1 by moles, methanol/water = 2 by volume) and 250 mg catalyst were added to the reactor. The reactor was first pressurized to 200 psig with helium and then depressurized, repeating three times to replace all air in the reactor while checking the reactor for leaks. Next, the reactor was pressurized to 500 psig, heated to 120 °C, and purged with additional helium to maintain the reaction pressure at 750 psig. The reaction was kept at 120 °C for 48 h and was sampled every 6–8 h (about 1 mL per sample) from the sampling port during the run. The samples were diluted ten times by methanol and filtered by using a syringe filter before analysis. After the first run, the reactor was cooled in an ice bath. The spent catalysts were collected by vacuum filtration and washed thoroughly with methanol. After drying in air, the spent catalyst was placed into the reactor for a second run under the exact same operating conditions.

An additional experiment was designed to test if any homogeneous reaction occurred due to leached chemicals from the catalyst. The catalyst was first refluxed at the reaction temperature in water for 2 h and was quickly filtered at that temperature. Next, the exact amount of reactants and methanol to maintain the methanol/water volumetric ratio of 2 as we did in the stability test were added. The mixture underwent the reaction at 120 °C for 48 h and sampled every 4–8 h.

The reactants and their condensation products were identified by gas chromatography/mass spectrometry (GC/MS; Shimadzu GC/MS-2100 with a DB-5 column from Alltech) if practical or by ^{1}H NMR and analyzed by HPLC (Shimadzu, with an SPD-20AV UV detector and a reverse phase C-18 column from Agilent). The monomer and dimer standards were prepared by NaOH catalyzed aldol condensation at room temperature and purified by chromatography. Furfural and HMF were analyzed at UV wavelength of 254 nm and the monomer/dimer products were analyzed at a UV wavelength of 330 nm; acetone and propanal are transparent to ultraviolet light. The side products are difficult to identify since both the reactant (furfural or HMF) and aldol products are bio-degradable. Some of the degradation products are insoluble in methanol. Therefore, the performance of the catalysts was evaluated only based on the disappearance of furfural (or HMF) and the selectivity to aldol products. The definitions are as follows:

$$\text{furfural disappearance (\%)} = \frac{\text{moles of furfural consumed}}{\text{moles of furfural input}} \times 100$$

$$\text{monomer selectivity (\%)} = \frac{\text{moles of monomer}}{\text{moles of furfural consumed}} \times 100$$

$$\text{dimer selectivity (\%)} = \frac{2 \times \text{moles of dimer}}{\text{moles of furfural consumed}} \times 100$$

selectivity of aldol product (%)

$$= \frac{\text{moles of monomer} + 2 \times \text{moles of dimer}}{\text{moles of furfural consumed}} \times 100$$

$$= \text{monomer selectivity} + \text{dimer selectivity}$$

$$\text{monomer yield (\%)} = \frac{\text{moles of monomer}}{\text{moles of furfural input}} \times 100$$

$$\text{dimer yield (\%)} = \frac{\text{moles of dimer}}{\text{moles of furfural input}} \times 100$$

For the product distribution:

$$\text{monomer (\%)} = \frac{\text{moles of monomer}}{\text{moles of monomer} + \text{moles of dimer}} \times 100$$

$$\text{dimer (\%)} = \frac{\text{moles of dimer}}{\text{moles of monomer} + \text{moles of dimer}} \times 100$$

2.3. Characterization

X-ray diffraction (XRD) patterns were measured with a Philips X'Pert professional diffractometer using a Cu Kα source with a wavelength of 1.54 Å. An accelerating voltage of 45 kV and a current of 40 A were used. A slit width of 0.5° was used on the source. Scans were collected using an X'Celerator detector.

The high resolution Ar adsorption isotherms of NaY and Nit-NaY were conducted at Quantachrome Laboratories using commercially available Autosorb instruments. The raw data was reduced by using the Autosorb software (version 1.53, Quantachrome instrument). The BET surface areas and micropore volumes of NaY and Nit-NaY were calculated by multipoint BET method and Vt-method in the relative pressure range of 0.02–0.3, respectively. The BET surface areas of the fresh and spent MgO–ZrO$_2$ catalyst were calculated by using multipoint BET method of the N$_2$ adsorption isotherms in the relative pressure range of 0.01–0.5. The pore size distributions of NaY and Nit-NaY were obtained by DFT method using a built-in DFT kernel (Ar at 87K-Zeolite/Silica: Cylinder, pore, NLDFT ads. branch model).

Carbon dioxide chemisorption and temperature programmed desorption (TPD) were conducted by a thermo-gravimetric analyzer (TA Instruments, SDTQ600) combined with a mass spectrometer (eXtorr Inc.) operating at 10^{-5} Torr. In a typical run, approximately 30 mg of the fresh or spent catalyst was placed into an alumina sample container, weighed, and equilibrated at 50 °C. The sample was then heated to 300 °C under 100 mL/min helium for 1 h with a 10 °C/min ramp to degas and then cooled to 50 °C until steady weight was established. The second gas, CO$_2$, was introduced into the chamber with a flow rate of 60 mL/min for about 3 h. After chemisorption equilibrium was established, the CO$_2$ flow was stopped and the physically adsorbed CO$_2$ was removed under helium flow until no further weight change was observed. Next, the sample was heated from 50 °C to 800 °C with a heating rate of

20 °C/min and maintained at 800 °C for 40–80 min. The CO_2 mass spectrum for the effluent was simultaneously monitored. The background control experiments were conducted in helium (without the CO_2 adsorption step) for calculation of the weight loss due to the decomposition of the catalyst itself. For the spent MgO–ZrO$_2$ catalyst, an additional run was conducted in which the catalyst was first calcined in a flow of air at 600 °C for 1 h, followed by CO_2 chemisorption and TPD with the same procedure as above to evaluate the change of basic sites after two runs of the aldol reaction at 120 °C for a total 91 h. The CO_2 uptake was calculated based on both the weight changes during chemisorption and TPD. The weight gain due to CO_2 chemisorption was equal to the weight difference before chemisorption and after the release of the physically adsorbed CO_2. The weight loss due to the CO_2 TPD was equal to the difference of total weight loss during TPD between samples with and without the CO_2 chemisorption step. The CO_2 uptakes were also calculated based on the CO_2 desorption peak from the mass spectra. The peak areas were calibrated by using 1 mL STP CO_2 of a standard volume loop.

Basic site titration was conducted under inert (helium) atmosphere according to the method used by Vidruk et al. [49]. Typically, catalyst powder (50 mg) was placed into a flask containing 50 mL o-xylene with 0.1 wt.% phenolphthalein and stirred at room temperature for 4 h in helium. The mixture was then titrated with 0.01 M benzoic acid in o-xylene until the color changed from colorless to pink. The concentration of basic sites was calculated based on the amount of acid consumed. The inert atmosphere was used here in order to avoid the error introduced by CO_2 in air.

The ^{29}Si single-pulse (SP) magic angle spinning (MAS) nuclear magnetic resonance (NMR) analysis of the fresh Nit-NaY and spent Nit-NaY was performed on a Varian 360 MHz spectrometer with 4 mm probe using 14 kHz MAS. A 90° pulse length of 2.4 μs was used with a recycle delay of 30 s, as established in our previous experiments [22]. The chemical shifts reported are with respect to neat liquid tetramethylsilane (TMS) at 0 ppm.

3. Results

3.1. Catalyst characterization

3.1.1. Powder XRD and high resolution adsorption isotherm
Fig. 1 shows the XRD patterns of NaY, Nit-NaY and the spent Nit-NaY. Nit-NaY retained all the reflection peaks of NaY, indicating the FAU structure was maintained after treatment in ammonia flow at 850 °C for 24 h. However, the intensities of the reflections over Nit-NaY were significantly reduced compared to that of NaY, indicating reduced crystallinity, consistent with our previous reports [21,22]. The percentage of crystalline material remaining in Nit-NaY can be estimated according to the method introduced by Solache et al.
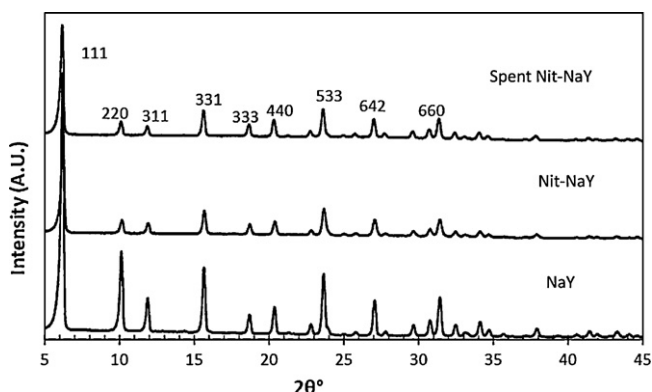

Fig. 1. The powder XRD patterns of NaY, Nit-NaY and the spent Nit-NaY.
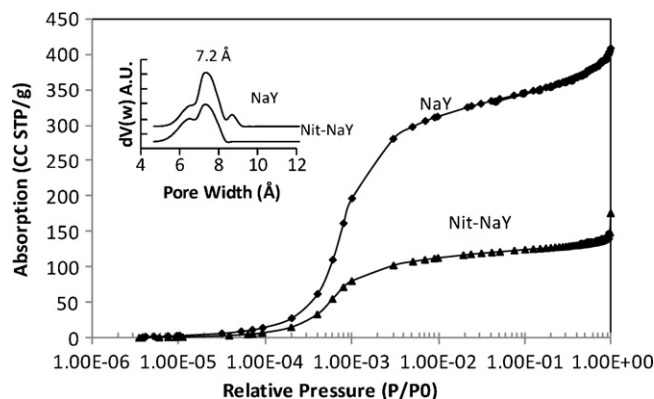

Fig. 2. The high resolution Ar adsorption isotherms and the pore size distribution of NaY and Nit-NaY. The results indicate that the Nit-NaY catalyst maintains pore size distribution and part of the crystal structure with the loss of pore volume and surface area to a degree. The unit of $dV(w)$ is cm^3/Å/g.

[50]. Here, the cystallinity of Nit-NaY was about 52% based on a comparison of the reflection peak areas of (5 3 3), (6 4 2), and (6 6 0) between NaY and Nit-NaY. In addition, a significant reduction of the intensity ratio of the reflections corresponding to (2 2 0) and (3 1 1) was observed, which is caused by the substitution of nitrogen into the zeolite framework [22]. There were no further structural changes in the spent Nit-NaY after reaction at 120 °C for 75 h in a methanol–water solvent. Fig. 2 shows the Ar isotherms of NaY and Nit-NaY and the corresponding pore size distributions. NaY and Nit-NaY present similar isotherms. The pore size of 7.2 Å for NaY was maintained over Nit-NaY. However, the Ar adsorption of Nit-NaY is less than that of NaY, indicating the reduction of the porosity. Micropore volumes (Vt-method) of NaY, Nit-NaY and the spent Nit-NaY are 0.36 mL/g, 0.13 mL/g and 0.17 mL/g (N$_2$ adsorption), respectively. The BET surface areas of NaY, Nit-NaY and the spent Nit-NaY are 954 m^2/g (C_{BET} = −45), 337 m^2/g (C_{BET} = −4.3) and 368 m^2/g (C_{BET} = −41, N$_2$ adsorption), respectively. Although the BET equation is not valid for these microporous materials, this shows the relative reduction of surface area of ∼2/3, similar to the micropore volume. The results from the high resolution Ar adsorption isotherm and XRD are consistent, showing that Nit-NaY maintains only part of the crystal structure, contributing to the reduction of the surface area, micropore volume, and crystallinity.

The XRD pattern of the calcined MgO–ZrO$_2$ catalyst (as seen in the supplementary materials Fig. S1) shows two phases, corresponding to cubic MgO and tetragonal ZrO$_2$, respectively. After reaction, the catalysts underwent a phase transition, where the spent MgO–ZrO$_2$ contained Mg(OH)$_2$ and ZrO$_2$. ZrO$_2$ retained high crystallinity without noticeable changes in the spent catalyst, while the Mg(OH)$_2$ showed broad XRD peaks, indicative of poor crystallinity. The BET surface area of the fresh MgO–ZrO$_2$ is 102 m^2/g and increased to 194 m^2/g for the spent MgO–ZrO$_2$, which might be attributed to a phase transition (MgO to Mg(OH)$_2$) or a roughening from the fresh catalyst to the spent catalyst.

3.1.2. Characterization of basic sites by CO_2-TPD and titration
Fig. 3 shows the CO_2 TPD-MS profiles over the fresh and spent MgO–ZrO$_2$ catalysts. The spent MgO–ZrO$_2$ was collected after two runs of furfural condensation with acetone at 120 °C for 91 h and washed with excess methanol. It was seen that the spent MgO–ZrO$_2$ after regeneration has almost the same amount of CO_2 uptake at 190 °C compared with the fresh MgO–ZrO$_2$ catalyst. The spent MgO–ZrO$_2$ showed only a very weak CO_2 uptake peak at 120 °C, but a sharp CO_2 peak at 400 °C related to the decomposition of adsorbed furfural and its degradation products, and a broad peak at 800 °C probably due to coke. There was a very small CO_2 peak at
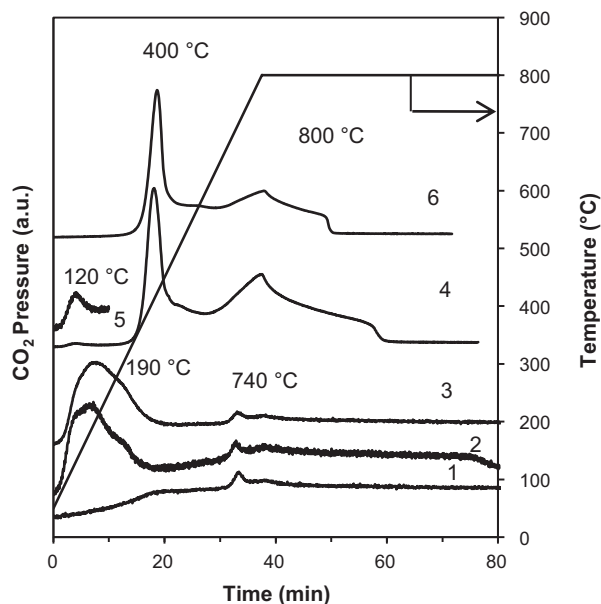
Fig. 3. CO_2 TPD-MS profiles over the fresh and spent MgO–ZrO$_2$ catalyst. Key: 1. Fresh MgO–ZrO$_2$, background control experiment; 2. Fresh MgO–ZrO$_2$; 3. Spent MgO–ZrO$_2$ calcined at 600 °C for 1 h; 4. Spent MgO–ZrO$_2$; 5. Spent MgO–ZrO$_2$, signal at low temperature; 6. Spent MgO–ZrO$_2$, background control experiment. The signals in Spectra 1, 2, 3 and 5 were multiplied by ten.

Fig. 4. CO_2 TPD-MS profiles over NaY, Nit-NaY and spent Nit-NaY. Key: 1. Fresh Nit-NaY, background control experiment; 2. Fresh NaY, background control experiment; 3. Fresh Nit-NaY; 4. Fresh NaY; 5. Spent Nit-NaY; 6. Spent Nit-NaY, background control experiment.

740 °C (in Thermograms 1–3), which might be due to the decomposition of magnesium or zirconium carbonate compounds formed after exposing the catalyst to air.

Fig. 4 shows the CO_2 TPD-MS profiles of NaY, Nit-NaY and the spent Nit-NaY. The spent Nit-NaY catalyst was collected after two runs of furfural condensation with acetone at 120 °C for 75 h and washed with excess methanol. The fresh Nit-NaY (in Thermogram Curve 3) shows two types of CO_2 desorption sites: one at low temperature near 150 °C and the other at high temperature above 800 °C. Since the high temperature CO_2 desorption was also observed on the fresh NaY, it might be related to the decomposition of carbonate compounds, for instance, Na$_2$CO$_3$, formed during CO_2 chemisorption. The low temperature CO_2 peaks at 150 °C over fresh NaY and spent Nit-NaY were very broad or absent, indicating the lack of the same kind of basic sites. In addition to the CO_2 desorption peaks, the CO_2 partial pressure increased continuously (almost linearly) from 200 °C to 800 °C during CO_2 TPD. The spent Nit-NaY catalyst showed two CO_2 uptake peaks at 550 °C and 740 °C. Again, these two peaks are associated with adsorbed furfurals, reaction intermediates, and/or the degradation products, respectively. The
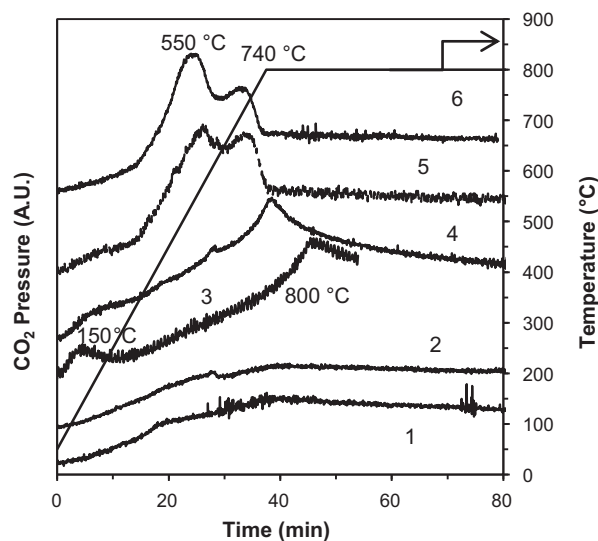
amount of adsorbed species over the spent Nit-NaY was much less than that adsorbed by the spent MgO–ZrO$_2$.

The results from CO_2-TPD–TGA (Figs. S2 and S3) are consistent with those from CO_2-TPD-MS experiments. In addition, the fresh Nit-NaY showed good stability toward heat with the weight loss similar to NaY during the background control experiment.

The CO_2 uptakes calculated from the TGA weight changes during CO_2 chemisorption and TPD and the CO_2 uptakes from CO_2-MS peaks over the fresh and spent catalyst are listed in Table 1, respectively. The CO_2 uptake over the fresh MgO–ZrO$_2$ and the spent MgO–ZrO$_2$ after calcination at 600 °C for 1 h are very close, indicating that the catalyst is regenerable. The spent MgO–ZrO$_2$ without calcination shows only about 10% CO_2 uptake. The CO_2 uptake capacities based on both the adsorption and desorption from TGA results are very close for all three zeolite samples, probably due to the ability of the zeolite cage to capture CO_2. The amount of basic sites over Nit-NaY was also calculated based on the CO_2 TPD-MS, which was about one order of magnitude smaller than that of the fresh MgO–ZrO$_2$. However, due to the desorption of the captured CO_2 over a broad temperature range, the baseline of TPD-MS over the zeolite samples shifted dramatically, thus making the method less accurate for quantification of basic sites of Nit-NaY.

The concentrations of basic sites calculated by titration are also shown in Table 1. The values are comparable to the results from

Table 1

The concentration of basic sites for fresh and spent catalysts from (1) CO_2 adsorption calculated from the TGA weight change, (2) C$_2$ desorption calculated by TGA weight change and TPD-MS area and (3) benzoic acid titration.

Catalyst	CO_2 adsorption		CO_2 uptake (basic sites concentration) $\times 10^4$ (mmol/mg catalyst)			
	Temperature	Time	Adsorption	Desorption		Titration
			By weight change	By weight change	By TPD-MS	
MgO–ZrO$_2$						
Fresh	50 °C	3 h	5.92	5.27	6.31	4.33
Spent	50 °C	3 h	0.68	0.43	0.64	0.65
Spent[a]	50 °C	3 h	6.47	5.76	6.05	–
Nit-NaY						
Fresh	50 °C	3 h	3.22	3.26	0.45	0.42
Spent	50 °C	3 h	3.62	3.61	–	–
NaY						
Fresh	50 °C	3 h	3.64	3.82	–	–

[a] The spent MgO–ZrO$_2$ catalyst calcined in air at 600 °C for 1 h before CO_2 adsorption.
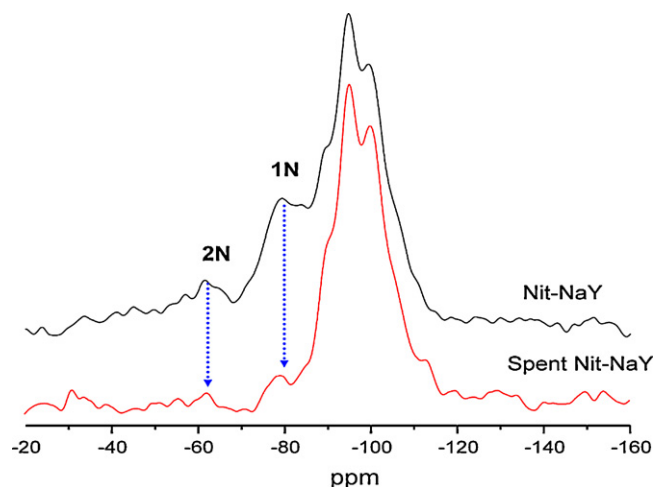
Fig. 5. ^{29}Si MAS NMR over the fresh and spent Nit-NaY catalyst. The spent Nit-NaY after two runs of furfural condensation with acetone at 120 °C for 75 h lost 90% of nitrogen in zeolite framework.

Fig. 6. Furfural disappearance, selectivity to aldol products, and product distribution for aldol condensation of furfural with acetone over MgO–ZrO$_2$, NaY and Nit-NaY. Reaction conditions: temperature: 120 °C; pressure: 750 psig of helium; reaction time: 24 h; total organic in solvent: 5 wt.%; furfural:acetone = 1 by moles; catalyst: 15 mg; solvent: water/methanol = 1 by volume.

either TGA or TPD-MS. However, the method could not be applied to quantify the basic sites of NaY or the spent Nit-NaY either, since the pH indicator was insufficient to show the color change.

3.1.3. ^{29}Si MAS NMR

Fig. 5 shows the ^{29}Si SP MAS NMR spectra of the fresh and the spent Nit-NaY catalyst. The TO$_4$ units in the zeolite become TO$_{4-x}$N$_x$ after nitrogen substitution (T: Si or Al). The symbol x refers the number of nitrogen atoms bonded to a central silicon (or aluminum) atom. The detailed quantum chemical calculations of chemical shifts for all possible Si–N environments for NaY and HY are given in our previous publication [22]. The resonances with chemical shifts at −73 and −82 ppm could be assigned to 1N environments (i.e., x = 1) and the resonance with chemical shifts at −58 and −64 ppm could be assigned to the 2N environments (i.e., x = 2). No 3N environments were observed for the fresh Nit-NaY sample. After reaction, the resonance assigned to the 2N environments disappeared and the intensity of the 1N resonance was decreased. The spectra were deconvoluted so as to extract the intensities of the different resonances, and thus the concentrations of the different local environments of TO$_{4-x}$N$_x$. The deconvolution was performed by considering the calculated and experimental chemical shift values for nitrogen substituted TO$_4$ units reported. The N content of the sample could then be estimated from these concentrations, as discussed in our earlier paper [22]. The analysis revealed that the nitrogen content decreased from 10% to 1% for the spent Nit-NaY. Therefore, a significant loss of substituted nitro-
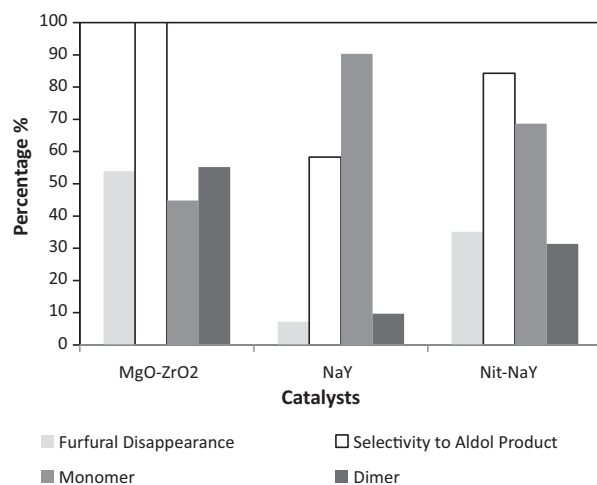
gen occurred after two runs of furfural condensation with acetone in a methanol–water solution.

3.2. Reactions

3.2.1. Aldol condensation reactions

MgO–ZrO$_2$, Nit-NaY and NaY were evaluated for the condensation of furfural and HMF with acetone or propanal. The reactions were carried out in the liquid phase at 120 °C in 750 psig of He for 16 h or 24 h under vigorous stirring in a high throughput batch reactor. The furfural (or HMF) and acetone (or propanal) molar ratio was kept at 1. The total organic content of the feed was 5 wt.%. The solvent was a 1:1 volumetric mixture of water and methanol. The amount of catalyst used was about 1/6 of the total organics by weight (about 15 mg).

Fig. 6 shows the catalytic performance of the aldol condensation of furfural with acetone over MgO–ZrO$_2$, NaY and Nit-NaY. The results of furfural/propanal, HMF/acetone, and HMF/propanal condensation reactions over these catalysts are listed in Table 2. The catalytic performance was evaluated by the disappearance of furfural, the selectivity to aldol products, and monomer or dimer distribution. In all experiments, there was no acetone self condensation product observed. There was also no furfural (or HMF)/propanal dimer observed as products. MgO–ZrO$_2$ had the highest activity and selectivity to the aldol products. NaY exhibited weak basicity with the lowest conversion. Nit-NaY showed dra-

Table 2
The performance of aldol condensation reactions of furfural (or HMF) with acetone (or propanal) over MgO–ZrO$_2$, NaY and Nit-NaY. Reaction conditions: temperature: 120 °C; pressure: 750 psig of helium; total organics in solvent: 5 wt.%; furfural:acetone = 1 by moles; catalyst: 15 mg; solvent: water/methanol = 1 by volume.

Reaction	Reactant (1:1 by molar)	Catalyst	Reaction time (h)	Disappearance of furfurals (%)	Selectivity to aldol products (%)	Distribution (%)	
						Monomer	Dimer
1	HMF/acetone	MgO–ZrO$_2$	16	51.4	91.9	56.5	43.5
2	HMF/acetone	NaY	16	14.1	89.7	85.9	14.1
3	HMF/acetone	Nit-NaY	16	40.1	80.9	72.7	27.3
4	Furfural/propanal	MgO–ZrO$_2$	16	60.4	90.0	100	–
5	Furfural/propanal	NaY	16	6.7	38.6	100	–
6	Furfural/propanal	Nit-NaY	16	55.5	104.7	100	–
7	HMF/propanal	MgO–ZrO$_2$	16	86.8	57.0	100	–
8	HMF/propanal	NaY	16	26.4	39.6	100	–
9	HMF/propanal	Nit-NaY	16	86.4	53.7	100	–

Note: The performance of furfural condensation with acetone is shown in Fig. 9. The experiment error is about 5%.

matically increased activity and selectivity to the aldol products compared to NaY. In the condensation of furfural with acetone as shown in Fig. 6, the furfural disappearances over MgO–ZrO$_2$, NaY and Nit-NaY were 59.9%, 7.2% and 35.1%, respectively. Among the consumed furfural, there were about 100%, 58.3% and 84.3% reacted to form aldol products. The unbalanced furfural was probably due to undetected intermediates [46], the degradation products from either furfural or monomer and dimer, or the chemical species that adsorbed on the catalyst surface including coke. It was seen that NaY had the highest ratio of monomer to dimer of about 9. However, the total yield of monomer is very low (3.5%) due to the low conversion and aldol product selectivity. The ratio of monomer to dimer over Nit-NaY was lower than that observed for NaY at about 2.2. However, it was significantly higher than that observed for MgO–ZrO$_2$ at 0.8.

The catalytic performance of HMF and acetone condensation over MgO–ZrO$_2$, NaY and Nit-NaY was similar to that of furfural and acetone condensation as seen in Table 2. Again, MgO–ZrO$_2$ had the highest catalytic activity and aldol product selectivity. Ninety two percent of the consumed HMF formed the aldol products with 56.5% of monomer and 43.5% of dimer. NaY showed the lowest activity with 14.1% of HMF disappearance, but this catalyst selectively produced monomer over dimer. The activity of Nit-NaY was comparable to MgO–ZrO$_2$ with about 40.1% of HMF conversion and 80.9% aldol product selectivity. The ratio of monomer to dimer was 2.7, higher than that of MgO–ZrO$_2$ which was 1.3. In the aldol condensation of furfural/HMF with propanal, the catalytic behavior of MgO–ZrO$_2$ and Nit-NaY was similar, showing much greater activity and selectivity towards aldol product than NaY.

In summary, incorporation of nitrogen into the framework of NaY increased the catalytic activity of Nit-NaY dramatically. The catalytic activities over Nit-NaY for the aldol condensation reactions of furfural/HMF with acetone/propanal were comparable to MgO–ZrO$_2$, but more selective towards the furfurals acetone monomer. The related catalytic activity over the studied catalysts follows the order: MgO–ZrO$_2$ > Nit-NaY > NaY.

3.2.2. Effect of water

Fig. 7 shows the solvent effect on the aldol condensations of furfural with acetone over MgO–ZrO$_2$ and Nit-NaY with water content varying from 100 vol.% to 25 vol.% in methanol–water solvents. With decreasing water content from 100 vol.% to 67 vol.%, the furfural disappearance decreased from 91% to 50% over MgO–ZrO$_2$ catalyst. However, the overall aldol product selectivity increased and the ratio of monomer to dimer slightly increased from 0.55 to ~0.8. Further decreasing the water content to less than 67 vol.% produced no obvious change of either furfural disappearance (≈50%) or the aldol product selectivity (100%), while, the selectivity of monomer to dimer varied slightly from 0.7 to 1.1. The average monomer and dimer yields were approximately 15% and 20%, respectively. However, the catalytic performance over Nit-NaY varied significantly with water content in the solvent. The furfural disappearance decreased dramatically from 75% to 20% by decreasing the water content from 100 vol.% to 25 vol.%. The ratio of monomer to dimer varied from 0.65 in pure water to 6.5 in 25 vol.% water. After decreasing water content to less than 50 vol.%, the monomer became the predominant product. Over the entire water to methanol ranges studied, the aldol product selectivity over Nit-NaY was maintained at 90%.

The effect of water on aldol condensations of HMF with acetone was also studied over MgO–ZrO$_2$ and Nit-NaY. The results were summarized in Table 3. Similarly, there was no preference to HMF acetone monomer or dimer over MgO–ZrO$_2$, but, decreasing water content to 67 vol.% generated more HMF acetone monomer than dimer over Nit-NaY. Therefore, water plays a significant role in the liquid phase aldol condensation reactions, especially the reac-
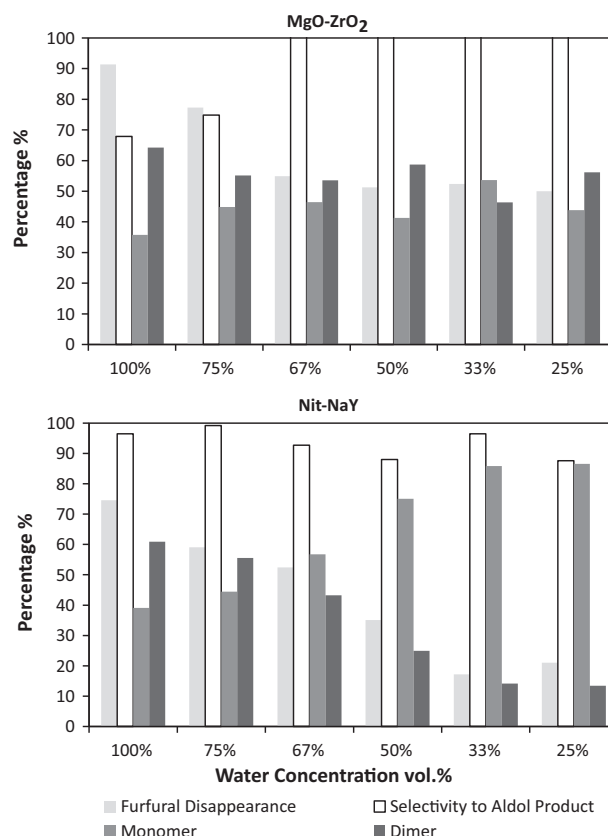

Fig. 7. Solvent effect on furfural disappearance and the product distribution over MgO–ZrO$_2$ and Nit-NaY. Reaction conditions: temperature: 120 °C; reaction time: 24 h; total organic in solvent: 5 wt.%, furfural/acetone = 1 by molar; catalyst: 1/6 total organics by weight (15 mg); solvent: variation of methanol to water volumetric ratios.

tions carried out over Nit-NaY. Water changes not only the catalytic activity, but also the product distribution.

3.2.3. Effect of feed concentration

Fig. 8 shows the effect of feed concentration on the catalytic performance of furfural and acetone condensation over MgO–ZrO$_2$ and Nit-NaY. The reactions were conducted at a constant furfural/acetone molar ratio of 1, total organics/catalyst weight ratio of 6, and methanol/water volumetric ratio of 1. Increasing the feed concentration increased the furfural disappearance and the tendency to generate more dimer product over MgO–ZrO$_2$. The furfural disappearance increased from 23% to 40% to 57% to 65% with feed concentrations of 1, 5, 8, and 15 wt.%, respectively. Meanwhile, the ratio of monomer to dimer decreased from 5.7 to 0.96 to 0.67 to 0.35, respectively. Increasing the feed concentration from 1 wt.% to 15 wt.% also gradually increased the furfural disappearance over Nit-NaY from 14% to 56%. However, the selectivity of monomer to dimer exhibited quite a different trend from that over MgO–ZrO$_2$. At a very low feed concentration of 1 wt.% over Nit-NaY, the monomer was the predominant aldol product and the ratio of monomer to dimer in the aldol products was as high as 24. At feed concentrations above 5 wt.%, the change in the ratio of monomer to dimer decreased, varying from 3 to 2.5 to 2 at concentrations of 5, 8, and 15 wt.%, respectively. Therefore, increasing the feed concentration increased the disappearance of furfural and the selectivity to dimer over both catalysts. However, Nit-NaY maintained a higher selectivity to monomer product at all feed concentrations through shape selectivity.

Table 3
Summary of solvent effect and catalyst to feed ratio effect over MgO–ZrO$_2$ and Nit-NaY. Reaction conditions: temperature: 120 °C; pressure: 750 psig of helium; total organics in solvent: 5 wt.%; furfural:acetone = 1 by moles.

Run#	Catalyst	Org/Cat (wt.)	Solvent (vol.)	Reaction time	Reaction temperature (°C)	Furfural (or HMF) disappearance (%)	Selectivity to aldol product (%)	Product distribution (%)	
								Monomer	Dimer
Reactant: HMF/acetone									
1	MgO–ZrO$_2$	6	Water	16 h	120	93.3	55.9	50.4	49.6
2	MgO–ZrO$_2$	6	Water/methanol = 2:1	16 h	120	68.5	84.5	48.6	51.4
3	MgO–ZrO$_2$	6	Water/methanol = 1:1	16 h	120	41.2	82.2	55.9	44.1
4	MgO–ZrO$_2$	6	Water/methanol = 1:2	16 h	120	38.6	81.1	67.8	32.2
5	Nit-NaY	6	Water	16 h	120	92.0	74.8	48.2	51.8
6	Nit-NaY	6	Water/methanol = 2:1	16 h	120	51.4	82.5	63.6	36.4
7	Nit-NaY	6	Water/methanol = 1:1	16 h	120	34.3	75.0	72.0	28.0
8	Nit-NaY	6	Water/methanol = 1:2	16 h	120	34.1	75.1	77.2	22.8
Reactant: furfural/acetone									
9	MgO–ZrO$_2$	60	Water/methanol = 1:1	24 h	120	32.9	106.1	54.1	45.9
10	MgO–ZrO$_2$	30	Water/methanol = 1:1	24 h	120	36.4	102.3	50.7	49.3
11	MgO–ZrO$_2$	18	Water/methanol = 1:1	24 h	120	47.8	100.5	45.0	55.0
12	MgO–ZrO$_2$	12	Water/methanol = 1:1	24 h	120	51.8	102.3	41.9	58.1
13	MgO–ZrO$_2$	6	Water/methanol = 1:1	24 h	120	53.9	103.5	44.8	55.2
14	MgO–ZrO$_2$	3	Water/methanol = 1:1	24 h	120	56.7	95.4	45.6	54.4
15	MgO–ZrO$_2$	2	Water/methanol = 1:1	24 h	120	66.0	75.7	42.4	57.9
16	Nit-NaY	12	Water/methanol = 1:1	24 h	120	33.5	57.5	82.1	17.9
17	Nit-NaY	6	Water/methanol = 1:1	24 h	120	48.9	55.7	69.9	30.1
18	Nit-NaY	4	Water/methanol = 1:1	24 h	120	59.8	68.7	65.1	34.9
19	Nit-NaY	3	Water/methanol = 1:1	24 h	120	70.6	72.1	55.6	44.4
20	Nit-NaY	2	Water/methanol = 1:1	24 h	120	82.8	75.7	47.1	52.9
21	Nit-NaY	1	Water/methanol = 1:1	24 h	120	97.5	59.6	58.4	41.6

3.2.4. Effect of catalyst to feed ratio

The results of aldol condensation of HMF with acetone by variation of catalyst to feed ratio over MgO–ZrO$_2$ and Nit-NaY are shown in Fig. 9. In addition, tabulated data on furfural acetone condensa-
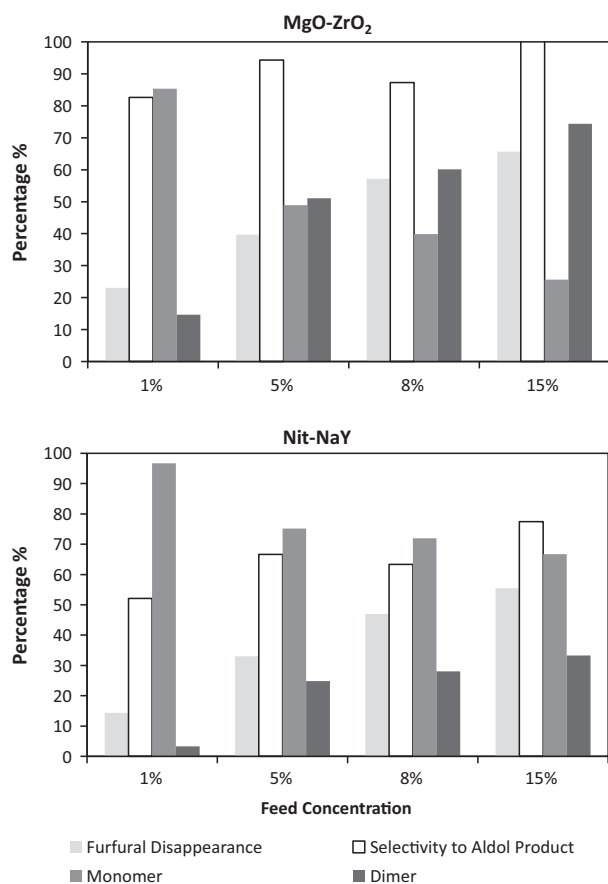

Fig. 8. Effect of feed concentration on furfural disappearance, aldol product selectivity and the product distribution over MgO–ZrO$_2$ and Nit-NaY. Reaction conditions: temperature: 120 °C; reaction time: 24 h; total organics/catalyst ratio of 6, furfural/acetone = 1 by moles; solvent: water/methanol = 1 by volume.
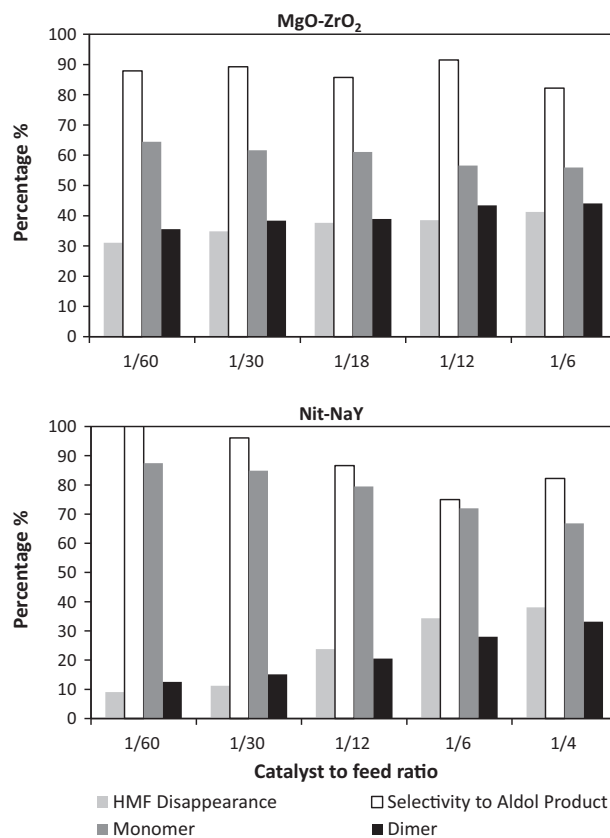

Fig. 9. Effect of catalyst to feed ratio by weight on the HMF disappearance, the selectivity to aldol products and the product distribution over MgO–ZrO$_2$ and Nit-NaY. Reaction conditions: temperature: 120 °C; reaction time: 16 h; total organics in solvent: 5 wt.%, HMF/acetone = 1 by moles; solvent: methanol/water = 1 by volume.

tion over these two catalysts is listed in Table 3 for comparison. The catalytic performance over MgO–ZrO$_2$ was independent of the catalyst to feed ratio (catalyst/total organics ranging from 1/60 to 1/6 by weight). The HMF disappearance slightly increased from 31% to 41% and the total aldol product selectivity was relatively unaffected at the level of 80% to 90%. The monomer to dimer ratio was slightly decreased with increase in catalyst amount. However, the HMF disappearance increased dramatically from 9% to 38% by changing the catalyst to feed ratio from 1/60 to 1/4 over Nit-NaY. The selectivity of monomer increased at the lower conversion on both catalysts. Nit-NaY displayed more selectivity to the monomer product over the entire range than that of the MgO–ZrO$_2$ catalyst. For furfural condensation with acetone as shown in Table 3, further increasing the catalyst to feed ratio to 1 resulted in almost 97.5% furfural disappearance over Nit-NaY. But, the higher the furfural disappearance, the lower the aldol selectivity (some of the degradation products could not be dissolved in methanol and hence partially contribute to the unbalanced furfural). There was no obvious preference for the monomer product at the increased catalyst to feed ratio of above 1/4 over Nit-NaY. The differences observed in the activity and selectivity between the two catalysts due to catalyst to feed ratio might indicate the different reaction mechanisms over these catalysts. It should also be noted that the ratio of monomer to dimer for HMF acetone condensation was higher than that for furfural acetone condensation over MgO–ZrO$_2$. This may be due to the relatively short reaction time for HMF acetone condensation reaction (16 h), which is insufficient to reach the reaction equilibrium as observed during the stability testing (Section 3.2.5).

3.2.5. Catalyst stability

Fig. 10 shows the time-on-steam (TOS) catalytic performance of MgO–ZrO$_2$ and Nit-NaY and their stability towards recycling for furfural/acetone condensation. The reactions were conducted in a Parr batch reactor as described in Section 2.3. The furfural disappearance increased from 12% at 1 h to 80% after about two days of reaction over the MgO–ZrO$_2$ catalyst. The selectivity to monomer increased initially from 13% at 1 h gradually to a maximum of 40% at 19 h, and then, slowly decreased to 24% at 44 h. The selectivity to dimer increased continuously from 4% at 1 h to 76% at 44 h. The selectivity to the aldol products and the product distribution during the time-on-stream (TOS) reaction are summarized and listed in Table 4. It was seen that the initial aldol products selectivity was as low as 17.3% and increased to about 100% with TOS at 19 h. The unbalanced furfural at the beginning of the reaction was presumably caused by undetected reaction intermediates. After catalyst recycling, the MgO–ZrO$_2$ catalyst retained most of the activity with only a slight decrease in dimer selectivity.

In contrast to MgO–ZrO$_2$, Nit-NaY displayed a different catalytic performance and stability for the aldol condensation reaction. In the first run, furfural disappearance increased with TOS from 37% at 0.5 h to 73% at 47 h. The selectivity to monomer increased from 9% at 0.5 h to around 40% at 10.5 h and remained constant until the end of the reaction. The selectivity to dimer increased at a relatively slow rate, starting at 2% at 0.5 h, increasing to 50% at 20.5 h, and gradually increasing to 60% after 47 h of reaction. The total selectivity to aldol products increased with TOS from 10% to about 100% in the period of 30 h reaction at 120 °C. In the second run, the furfural disappearance first decreased from 33% to 12% in the first 5 h of reaction then slowly increased from 11% to 21% after 30 h. In addition, the selectivity to dimer was relatively low, less than 2% in the entire TOS range, while, the selectivity to monomer increased from about 1% to 14%. During the first 5 h of reaction, there were trace amounts of monomer and dimer products observed despite the fact that the initial furfural disappearance was close to that of the first run. This abnormal behavior was reproducible and the reason is not understood at present. It is likely caused by adsorption
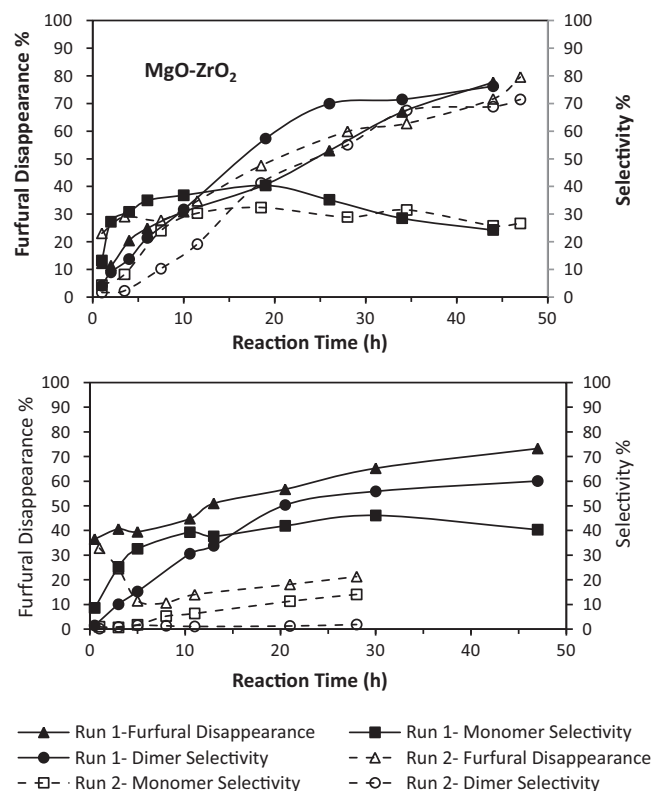

Fig. 10. TOS furfural disappearance and the selectivities to monomer and dimer over MgO–ZrO$_2$ and Nit-NaY. The second run was conducted by using the catalyst recycled from the first run. Reaction conditions: reaction volume: 75 mL; temperature: 120 °C; pressure: 750 psig of helium; total organics 5 wt.%, furfural/acetone = 1 by moles; solvent: methanol/water = 2; catalysts: 250 mg, about 1/12 total organics by weight.

of furfural onto the catalyst surface and/or the base strength of the spent Nit-NaY catalyst which was insufficient to initiate the reaction intermediates towards the aldol product (reversible reactions from furfural to the reaction intermediates) at the beginning of the reaction. The loss of the catalytic activity over the spent Nit-NaY in the long run was presumably due to the loss of basic sites (nitrogen in the framework). This is consistent with the characterization results from CO$_2$ TPD, benzoic acid titration and ^{29}Si SP MAS NMR in Sections 3.1.2 and 3.1.3.

4. Discussion

4.1. Shape selectivity

Shape selective zeolite catalysis was first reported by Weisz and co-workers in 1960 [51] in the petroleum industry and was later applied for the production of high-grade gasoline from biomass compounds [52,53]. Shape selective catalysis is defined as the transformation of reactants into products depending on how the processed molecules fit into the pore of a catalyst [54]. Here, we estimated the kinetic diameters and critical diameters of various molecules as listed in Table 5 in order to determine if shape selectivity is expected to occur within different sizes of zeolite pores. The methods of calculation of kinetic and critical diameter can be found in the supplementary materials.

The 12-ring widow size of zeolite Y is 7.4 Å [6]. The high resolution Ar adsorption isotherms show that the pore sizes of NaY and Nit-NaY are about 7.2 Å, intermediate to the sizes of furaldehyde acetone monomer and dimer. The size at the faujasite pore opening is sufficient to accommodate the monomer product but is too

Table 4

Summary of TOS furfural disappearance and aldol product distribution over MgO–ZrO$_2$ and Nit-NaY. Reaction was conducted in a Parr batch reactor at 120 °C in 750 psig of helium. Organics: furfural/acetone = 1, 5 wt.%; solvent: water/methanol = 2 by volume; catalysts: 1/12 of total organics by weight; reaction volume: 75 mL. The second run was conducted by using catalyst recycled from the first run.

| Reaction time (h)	Furfural disappearance (%)	Selectivity to aldol products (%)	Distribution (%)		Reaction time (h)	Furfural disappearance (%)	Selectivity to aldol products (%)	Distribution (%)	
			Monomer	Dimer				Monomer	Dimer
MgO–ZrO$_2$: first run					MgO–ZrO$_2$: second run				
1	12.2	17.3	86.7	13.3	1	23.1	6.0	84.1	15.9
2	11.4	36.1	85.9	14.1	3.5	29.1	10.6	87.8	12.2
4	20.4	44.5	81.8	18.2	7.5	27.8	34.4	82.4	17.6
6	24.9	56.7	76.7	23.4	11.5	34.8	49.5	76.0	24.0
10	30.9	68.5	69.6	30.1	18.5	47.6	73.7	61.1	38.9
19	40.7	97.6	58.5	41.5	28	59.9	84.0	51.2	48.8
26	52.9	105	50.2	49.8	34.5	62.8	99.0	48.3	51.7
34	66.9	99.9	44.4	55.6	44	71.6	94.7	42.8	57.2
44	77.6	100.4	38.9	61.1	47	79.6	98.1	42.7	57.3
Nit-NaY: first run					Nit-NaY: second run				
0.5	36.6	10.1	91.9	8.1	1	32.9	1.3	89.6	10.4
3	40.7	35.3	83.3	16.7	3	24.6	1.7	60.0	40.0
5	39.5	47.8	81.0	19.0	5	11.5	3.4	69.0	31.0
10.5	44.8	69.9	72.0	28	8	10.7	6.7	88.6	11.4
13	51.1	71.5	69.0	31.0	11	14.0	7.5	92.0	8.0
20.5	56.8	92.3	62.5	37.5	21	18.2	12.7	94.6	5.4
30	65.3	102.0	62.3	37.7	28	21.4	16.0	93.7	6.3
47	73.3	100.4	57.3	42.7					
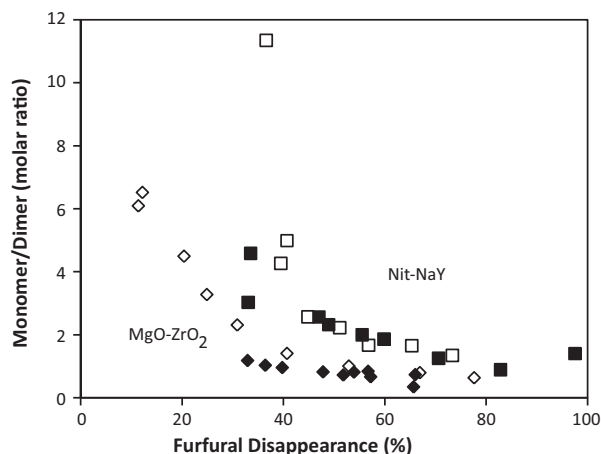
Fig. 11. Furfural disappearance as a function of molar ratio of furfural acetone monomer over dimer. The data are compared at methanol/water solvent volumetric ratio of 1 (solid symbols) and methanol/water volumetric ratio of 2 (open symbols).

Fig. 11 summarizes the furfural disappearance as a function of the molar ratio of monomer over dimer at the methanol/water solvent volumetric ratio of 1 and 2. It is clearly seen that the Nit-NaY was more selective towards monomer in the entire range of furfural disappearance than that of MgO–ZrO$_2$, thus evidence that the shape selectivity did occur over Nit-NaY. Further experiments showed that the shape selectivity to monomer over Nit-NaY was not affected by feed concentration, catalyst to feed ratio, and reaction time. However, the water content in the solvent has a dramatic effect on the selectivity over Nit-NaY. Since the Nit-NaY catalyst lost a significant degree of its FAU-type crystallinity and microporosity after nitrogen substitution, the significant amount of dimer we speculate is generated by the external surface reaction. In the future, the optimization of nitridation procedure should be performed in order to minimize the aldol dimer formation due to external surface reaction.

4.2. Effect of water

Water content in the solvent plays a significant role on the performance of both catalysts, especially for Nit-NaY. Increasing water content leads to a higher conversion and increased dimer selectivity on both MgO–ZrO$_2$ and Nit-NaY. On the one hand, the furfural/acetone dimer is not able to dissolve in the solvent with high water content, thus, the precipitation of dimer drives the reaction towards the generation of more dimer. On the other hand, the pores of the zeolite might be completely filled with water when using solvents with high water content in methanol. Therefore, the reaction takes place on the external zeolite surface, allowing dimer to be formed more easily.

small to allow the rapid diffusion of the dimer product, thus leading to a high selectivity towards the monomer product. In contrast, the fresh MgO–ZrO$_2$ shows a broad pore size distribution from 5 Å to 1000 Å, thus having no preference to monomer due to the catalyst texture. Here, NaY was specifically chosen as the starting material because Na$^+$ might lead to stronger basic strength after nitrogen substitution than HY [55].

Table 5

List of the kinetic diameters and critical sizes of the molecules of interest.

Molecule	Kinetic diameter (Å)	Critical size (Å)		Molecule	Kinetic diameter (Å)	Critical diameter (Å)	
		Width	Length			Width	Length
Furfural	5.7	4.56	5.99	HMF	6.2	5.42	8.64
FA monomer	6.3	4.87	9.89	HA monomer	6.8	4.97	12.15
FA dimer	7.4	6.03	13.75	HA dimer	8.0	6.66	17.95
FP monomer	6.3	5.24	8.64	HP monomer	6.8	5.22	10.90
FP dimer	6.9	5.54	10.81	HP dimer	7.2	6.71	12.91

Note: "FA" means furfural acetone; "FP" means furfural propanal; "HA" means HMF acetone; "HP" means HMF propanal.

4.3. Stability

In the stability test, MgO–ZrO$_2$ maintained its catalytic performance in the two reaction cycles. An additional experiment (as shown in the supplementary materials Fig. S5) shows that the predominate reaction occurred through heterogeneous catalysis over MgO–ZrO$_2$ despite the fact that a small amount of catalyst leached out into the hot solution under the reaction conditions. The leached catalyst underwent re-precipitation after cooling down to room temperature and could be easily recycled. A similar experiment was conducted by Barrett et al. [44], in which the MgO–ZrO$_2$ was recycled three times without any loss of catalytic activity, consistent with our experimental observation.

The stability of Nit-NaY was poor since more than two thirds of the activity was lost after a single catalytic reaction during the stability test. Silicon-29 SP MAS NMR further confirmed that the framework nitrogen in Nit-NaY was leaching out-about 90% loss occurred after two runs of furfural condensation with acetone at 120 °C for a total reaction time of 75 h. The leaching of nitrogen may be caused by hydrolysis of the nitrogen with water at elevated temperature. Agarwal et al. [56] conducted DFT calculations on the kinetic stability of HY, leading to the prediction that nitrogen-substituted HY remains stable at temperatures below 400 °C in saturated water loading in the HY unit cell (200 molecules of water per unit cell). However, the current experiment reveals that Nit-NaY is not stable in water–methanol solvent at 120 °C. This might be due to the extra-framework sodium cations or the competitive adsorption of water, methanol and reactants at the sites, driving the hydrolysis reaction to the lower temperature. This discrepancy could also arise from the fact that the sites that leach may not be precisely the same kind as those modeled by Agarwal et al. [56,57], prompting new DFT calculations on nitrogen-substituted NaY. The influence of water on the activity of nitridated NaX and NaY was studied previously by Ernst et al. [58]. It was reported that the uptake of water during storage and subsequent hydrolysis were responsible for the deactivation of the nitrogen substituted zeolites. The detrimental effect of water on the stability of nitrogen-substituted AlPO was also reported by Benítez et al. [59,60]. These observations of hydrolysis of the framework nitrogen occurred at room temperature. However, there was no evidence of the loss of catalytic activity over Nit-NaY in this study during the approximate six month storage period in desiccators without the protection of nitrogen.

4.4. The base strength and the nature of basic sites

Kelly et al. [61] summarized the base strength of the most studied solid base catalysts and the minimal base strength required to remove the proton from a R_1–CH_2–R_2 reactant molecule for the condensation reaction. It was reported that a strong base with pK_a of about 20 was required to deprotonate acetone and propanal. MgO is a strong solid base catalyst [61]. The basic sites on the MgO catalyst have been well studied [49,62,63]. The strongest sites are attributed to Lewis base sites of the low coordination (LC) surface oxygen; the second strongest basic sites are formed at acid-base pairs (Mg^{2+}–O^{2-}); the weakest base sites are the surface hydroxyl groups [62]. The CO$_2$ TPD-MS of MgO–ZrO$_2$ showed three desorption peaks at temperatures of 740 °C, 190 °C and 120 °C, which may be assigned to LC Lewis base sites, Mg^{2+}–O^{2-} pair and the surface hydroxyl groups, respectively. There was no observation of the extra desorption of CO$_2$ due to ZrO$_2$, which might be due to the low content of ZrO$_2$ in MgO–ZrO$_2$ at 1/18 by moles. The CO$_2$ desorption at 740 °C was due to the adsorption of CO$_2$ after exposing the LC Lewis base sites to air, forming carbonate species. Therefore, this peak was also observed on the fresh catalyst in the background control experiment. However, there are few of these strongest basic sites (0.36×10^{-4} mmol/mg catalyst from the cal-

culation of TPD-MS peak). Since these sites were all occupied by CO$_2$ after exposure to air, they are unlikely to be the catalytically active sites. The Brønsted base sites were generated due to the heterolytic dissociation of water at the surface of MgO. These sites were indistinguishable on the fresh and the spent catalyst after calcination, but very noticeable on the spent catalyst as seen in Fig. 3, indicating that these sites were formed during reaction. The XRD pattern of the spent MgO–ZrO$_2$ shows broad reflections assigned to Mg(OH)$_2$, providing further evidence for the formation of surface hydroxyl groups over MgO–ZrO$_2$. Even though the base strength of OH groups is considered to be lower than that of the O^{2-} ions on the MgO surface [64], they were reported to be active for aldol condensation of acetone [65].

The base strength of NaY is due to the negative charge densities of the framework oxygen atoms. Zhu et al. [24] reported that the pK_a value of NaY was less than 7.2. Here, NaY had very low activity in the furfural/acetone condensation reactions which is consistent with these previous studies and showed the weak base strength. The nitrided nanoporous materials have been reported to catalyze the reactions requiring mild to mediate base strength, including condensations of benzaldehyde with compounds containing a methylenic group such as malononitrile [17,40], ethyl cyanoacetate [38], and phenylsulfonyl-acetonitrile [66]. Replacing the oxygen with the less electronegative nitrogen increases the electron-donating tendency (Lewis base strength) of the lone pair on the bridging atom, which apparently increases the base strength from a pK_a value of less than 7.2 on NaY to a strong base on Nit-NaY [30]. The CO$_2$ TPD-MS of the fresh Nit-NaY showed a desorption peak at 150 °C, indicating that the base strength of the framework nitrogen on Nit-NaY is weaker than that of Mg^{2+}–O^{2-} pairs (190 °C), but stronger than that of Mg(OH)$_2$ (120 °C).

Climent et al. [67] conducted the aldol condensation reaction of heptanal with benzaldehyde over the nitrogen-substituted amorphous aluminophosphate (ALPO) and found the cooperative effect between week acid and base sites. The bi-functional acid-base mechanism was proposed, which involved the activation of benzaldehyde by protonation-polarization of the carbonyl group on the acid sites and the nucleophilic addition of the enolate heptanal intermediate generated on the basic sites. Similarly, we propose here that the driving force for the formation of enolate is the combination of the free electron pair and the condensed electronegative charge on the framework nitrogen, and the positively charged sodium cations (hard Lewis acid [68]) and/or the surface hydroxyl groups functioned as the site to activate furfural. The existence of surface silanol groups and Al(OH)$_2$ was confirmed by an initial FT-IR experiment as seen in the supplementary materials Fig. S4.

5. Conclusions

Aldol condensations of furaldehydes with acetone and propanal was studied on solid base catalysts MgO–ZrO$_2$, NaY and Nit-NaY. Nit-NaY showed catalytic activity comparable to MgO–ZrO$_2$ and much higher than that of untreated NaY. This indicates that replacing the bridging oxygen by less electronegative nitrogen increases the base strength of the zeolite framework dramatically. Nit-NaY showed more selectivity to monomer than MgO–ZrO$_2$ due to the small cage size in the FAU structure, indicating a shape selective base catalyst. The size at the faujasite pore opening is sufficient to accommodate the monomer product but is too small to allow the rapid diffusion of the dimer product. Increasing water concentration of the feed solution leads to increased catalyst activity and dimer selectivity on Nit-NaY. On MgO–ZrO$_2$, increasing the water content had no obvious effect on either furfural disappearance or dimer selectivity at low water concentration (less than 67 vol.%). Upon further increasing water concentration to above 75 vol.%, the catalytic activity and dimer selectivity increased. Increasing the

feed concentration increased the disappearance of furfural and the selectivity to dimer on both catalysts. Increasing the catalyst to feed ratio from 1/60 to 1/6 has no obvious effect over MgO–ZrO$_2$, but significantly increased the disappearance of furfurals and lowered the monomer to dimer ratio over Nit-NaY. Nit-NaY was more sensitive towards water and catalyst to feed ratio for the studied reactions compared to MgO–ZrO$_2$. Nit-NaY showed higher selectivity towards monomer than MgO–ZrO$_2$ in the entire range of furfural disappearance. Nit-NaY was found to be unstable in the water–methanol solvent with the loss in catalytic activity due to leaching of the framework nitrogen, while MgO–ZrO$_2$ showed good recyclability.

CO$_2$ TPD-MS and XRD distinguish three types of basic sites on MgO–ZrO$_2$, attributed to LC Lewis basic sites, Mg^{2+}–O^{2-} pairs and surface hydroxyl groups. The latter two sites are likely the catalytically active sites for liquid phase aldol condensation of furfurals with acetone/propanal. Due to the strong adsorption of CO$_2$ on NaY, CO$_2$ TPD-MS and CO$_2$ TPD–TGA are not deemed suitable to quantify the basic sites over Nit-NaY. Silicon 29 MAS NMR of the fresh and spent Nit-NaY disclosed that the substituted nitrogens are located in 1N or 2N environments, where one or two of oxygen atoms in TO$_4$ units were replaced by nitrogen. The base strength of Nit-NaY is in between of Mg^{2+}–O^{2-} pairs and Mg(OH)$_2$. The significant leaching of nitrogen from Nit-NaY during the aldol condensation in water–methanol solvent was observed.

These results provide the first clear evidence of shape selectivity in nitrogen-substituted zeolites. This proof-of-principle is an important step forward for providing a new tool in the arsenal of heterogeneous catalysis, especially as this field pursues solutions to problems in biomass refining and biofuel production. Further research is required to improve the stability and the selectivity of basic zeolites, either by modifying reaction conditions, solvents, nitridation methods, or the basic sites themselves.

Acknowledgements

Appendix A. Supplementary data

Supplementary data associated with this article can be found, in the online version, at doi:10.1016/j.apcata.2010.10.023.

References

[1] Y. Ono, T. Baba, Catal. Today 38 (1997) 321–337.
[2] Y. Ono, J. Catal. 216 (2003) 406–415.
[3] H. Hattori, Appl. Catal. A: Gen. 222 (2001) 247–259.
[4] A. Corma, S. Iborra, C.G. Bruce, K. Helmut, Adv. Catal. 49 (2006) 239–302.
[5] R.J. Davis, J. Catal. 216 (2003) 396–405.
[6] S.M. Auerbach, K.A. Carrado, P.K. Dutta (Eds.), Handbook of Zeolite Sicence and Technology, Marcel Dekker, New York, 2004.
[7] M. Huang, A. Adnot, S. Kaliaguine, J. Am. Chem. Soc. 114 (2002) 10005–10010.
[8] J. Zhu, Y. Chun, Y. Wang, Q. Xu, Catal. Today 51 (1999) 103–111.
[9] L.R.M. Martens, P.J. Grobet, W.J.M. Vermeiren, P.A. Jacobs, Stud. Surf. Sci. Catal. 28 (1986) 935–941.
[10] P.E. Hathaway, M.E. Davis, J. Catal. 116 (1989) 263–278.
[11] G.J. Suppes, M.A. Dasari, E.J. Doskocil, P.J. Mankidy, M.J. Goff, Appl. Catal. A: Gen. 257 (2004) 213–223.
[12] I. Rodriguez, S. Iborra, F. Rey, A. Corma, Appl. Catal. A: Gen. 194–195 (2000) 241–252.
[13] B.M. Choudary, M.L. Kantam, P. Sreekanth, T. Bandopadhyay, F. Figueras, A. Tuel, J. Mol. Catal. A: Chem. 142 (1999) 361–365.
[14] X. Zhang, E.S. Man Lai, R. Martin-Aranda, K.L. Yeung, Appl. Catal. A: Gen. 261 (2004) 109–118.
[15] K.-i. Shimizu, E. Hayashi, T. Inokuchi, T. Kodama, H. Hagiwara, Y. Kitayama, Tetrahedron Lett. 43 (2002) 9073–9075.
[16] A.-J. Han, H.-Y. He, J. Guo, H. Yu, Y.-F. Huang, Y.-C. Long, Micropor. Mesopor. Mater. 79 (2005) 177–184.
[17] S. Ernst, M. Hartmann, S. Sauerbeck, T. Bongers, Appl. Catal. A: Gen. 200 (2000) 117–123.
[18] K. Narasimharao, M. Hartmann, H.H. Thiel, S. Ernst, Micropor. Mesopor. Mater. 90 (2006) 377–383.
[19] J. Guo, A.-J. Han, H. Yu, J.-P. Dong, H. He, Y.-C. Long, Micropor. Mesopor. Mater. 94 (2006) 166–172.
[20] A.-J. Han, J. Guo, H. Yu, Y. Zeng, Y.-F. Huang, H.-Y. He, Y.-C. Long, ChemPhysChem 7 (2006) 607–613.
[21] K.D. Hammond, M. Gharibeh, G.A. Tompsett, F. Dogan, A.V. Brown, C.P. Grey, S.M. Auerbach, W.C. Conner Jr., Chem. Mater. 22 (2009) 130–142.
[22] F. Dogan, K.D. Hammond, G.A. Tompsett, H. Huo, W.C. Conner Jr., S.M. Auerbach, C.P. Grey, J. Am. Chem. Soc. 131 (2009) 11062–11079.
[23] K.D. Hammond, S.M. Auerbach, in: I. Halasz (Ed.), Silica and Silicates in Modern Catalysis, Research Signpost, Kerala, India, 2010.
[24] J.H. Zhu, Y. Chun, Q.-h. Xu, Y. Qin, Mater. Lett. 33 (1998) 331–335.
[25] Y. Xia, R. Mokaya, J. Phys. Chem. C 112 (2008) 1455–1462.
[26] C.W. Jones, K. Tsuji, M.E. Davis, Nature 393 (1998) 52–54.
[27] D. Lesthaeghe, V. Van Speybroeck, G.B. Marin, M. Waroquier, J. Phys. Chem. B 109 (2005) 7952–7960.
[28] A. Cauvel, D. Brunel, F. Di Renzo, P. Moreau, F. Fajula, in: H.K. Beyer, H.G. Karge, I. Kiricsi, J.B. Nagy (Eds.), Studies in Surface Science and Catalysis, Elsevier, 94, 1995, pp. 286–293.
[29] A. Corma, P. Viruela, L. Fernández, J. Mol. Catal. A: Chem. 133 (1998) 241–250.
[30] R. Astala, S.M. Auerbach, J. Am. Chem. Soc. 126 (2004) 1843–1848.
[31] J. EI Haskouri, S. Cabrera, F. Sapiña, J. Latorre, C. Guillem, A. Beltrán-Porter, D. Beltrán-Porter, M.D. Marcos, P. Amorós, Adv. Mater. 13 (2001) 192–195.
[32] Y. Xia, R. Mokaya, Angew. Chem. Int. Ed. 42 (2003) 2639–2644.
[33] C. Zhang, Q. Liu, Z. Xu, J. Non-Cryst. Solids 351 (2005) 1377–1382.
[34] N. Chino, T. Okubo, Micropor. Mesopor. Mater. 87 (2005) 15–22.
[35] J. Wang, Q. Liu, Micropor. Mesopor. Mater. 83 (2005) 225–232.
[36] M.J. Climent, A. Corma, V. Fornés, A. Frau, R. Guil-López, S. Iborra, J. Primo, J. Catal. 163 (1996) 392–398.
[37] X. Guan, F. Zhang, G. Wu, N. Guan, Mater. Lett. 60 (2006) 3141–3144.
[38] J. Xiong, Y. Ding, H. Zhu, L. Yan, X. Liu, L. Lin, J. Phys. Chem. B 107 (2003) 1366–1369.
[39] K.D. Hammond, F. Dogan, G.A. Tompsett, V. Agarwal, W.C. Conner, C.P. Grey, S.M. Auerbach, J. Am. Chem. Soc. 130 (2008) 14912–14913.
[40] C. Zhang, Z. Xu, K. Wan, Q. Liu, Appl. Catal. A: Gen. 258 (2004) 55–61.
[41] G.W. Huber, J.A. Dumesic, Catal. Today 111 (2006) 119–132.
[42] R. Xing, A.V. Subrahmanyam, H. Olcay, W. Qi, G.P. van Walsum, H. Pendse, G.W. Huber, Green Chem. 12 (2010) 1933–1946.
[43] J.N. Chheda, J.A. Dumesic, Catal. Today 123 (2007) 59–70.
[44] C.J. Barrett, J.N. Chheda, G.W. Huber, J.A. Dumesic, Appl. Catal. B: Environ. 66 (2006) 111–118.
[45] G.W. Huber, J.N. Chheda, C.J. Barrett, J.A. Dumesic, Science 308 (2005) 1446–1450.
[46] N. Fakhfakh, P. Cognet, M. Cabassud, Y. Lucchese, M.D. de Los Ríos, Chem. Eng. Process.: Process Intensification 47 (2008) 349–362.
[47] M.A. Aramendía, V. Borau, C. Jiménez, A. Marinas, J.M. Marinas, J.R. Ruiz, F.J. Urbano, J. Mol. Catal. A: Chem. 218 (2004) 81–90.
[48] M.A. Aramendía, V. Boráu, C. Jiménez, A. Marinas, J.M. Marinas, J.A. Navío, J.R. Ruiz, F.J. Urbano, Colloids Surf. A 234 (2004) 17–25.
[49] R. Vidruk, M.V. Landau, M. Herskowitz, M. Talianker, N. Frage, V. Ezersky, N. Froumin, J. Catal. 263 (2009) 196–204.
[50] M. Solache, I. García, P. Bosch, S. Bulbulian, A. Blumenfeld, J. Fripiat, Micropor. Mesopor. Mater. 21 (1998) 19–25.
[51] P.B. Weisz, V.J. Frilette, J. Phys. Chem. 64 (1960) 382–1382.
[52] P.B. Weisz, W.O. Haag, P.G. Rodewald, Science 206 (1979) 57–58.
[53] T.R. Carlson, T.P. Vispute, G.W. Huber, ChemSusChem 1 (2008) 397–400.
[54] B. Smit, T.L.M. Maesen, Nature 451 (2008) 671–678.
[55] V. Agarwal, G.W. Huber, W.C. Conner Jr., S.M. Auerbach, J. Phys. Chem. C, submitted for publication.
[56] V. Agarwal, G.W. Huber, W.C. Conner Jr., S.M. Auerbach, J. Catal. 270 (2010) 249–255.
[57] V. Agarwal, G.W. Huber, W.C. Conner Jr., S.M. Auerbach, J. Catal. 269 (2010) 53–63.
[58] S. Ernst, M. Hartmann, T. Hecht, P. Cremades Jaén, S. Sauerbeck, G.G.R. Aiello, F. Testa, Stud. Surf. Sci. Catal. 142 (2002) 549–556.
[59] J.J. Benítez, P. Malet, I. Carrizosa, J.A. Odriozola, R. Conanec, R. Marchand, Y. Laurent, J. Eur. Ceram. Soc. 17 (1997) 1979–1982.
[60] J.J. Benítez, A. Díaz, Y. Laurent, J.A. Odriozola, Appl. Catal. A: Gen. 176 (1999) 177–187.
[61] F. King, G.J. Kelly, Catal. Today 73 (2002) 75–81.
[62] V.K. Díez, C.R. Apesteguía, J.I. Di Cosimo, J. Catal. 240 (2006) 235–244.
[63] E. Knözinger, K.-H. Jacob, S. Singh, P. Hofmann, Surf. Sci. 290 (1993) 388–402.
[64] H. Kabashima, H. Hattori, Catal. Today 44 (1998) 277–283.
[65] G. Zhang, H. Hattori, K. Tanabe, Appl. Catal. 36 (1988) 189–197.
[66] M.J. Climent, A. Corma, R. Guil-Lopez, S. Iborra, J. Primo, Catal. Lett. 59 (1999) 33–38.
[67] M.J. Climent, A. Corma, V. Fornés, R. Guil-Lopez, S. Iborra, Adv. Syn. Catal. 344 (2002) 1090–1096.
[68] R.G. Pearson, J. Am. Chem. Soc. 85 (1963) 3533–3539.